Research article

Siyu Qian, Xinlong Chen, Shiyu Jiang, Qiwen Pan, Yachen Gao, Lei Wang, Wei Peng, Shanjun Liang, Jie Zhu* and Shengchun Liu*

Direct detection of charge and discharge process in supercapacitor by fiber-optic LSPR sensors

https://doi.org/10.1515/nanoph-2019-0504
Received December 5, 2019; revised January 23, 2020; accepted January 26, 2020

Abstract: Supercapacitors with high power density, ultralong lifespan and wide range operating temperature have drawn significant attention in recent years. However, monitoring the state of charge in supercapacitors in a cost-effective and flexible way is still challenging. Techniques such as transmission electron microscopy and X-ray diffraction can analyze the characteristics of supercapacitor well. But with large size and high price, they are not suitable for daily monitoring of the supercapacitors' operation. In this paper, a low cost and easily fabricated fiber-optic localized surface plasmon resonance (LSPR) probe is proposed to monitor the state of charge of the electrode in a supercapacitor. The Au nanoparticles were loading on the fiber core as LSPR sensing region. In order to implant the fiber in the supercapacitor, a reflective type of fiber sensor was used. The results show that this tiny fiber-optic LSPR sensor can provide online monitoring of the state of charge during the charging and discharging process *in situ*. The intensity shift in LSPR sensor has a good linear relationship with the state of charge calculated by standard galvanostatic charging and discharging test. In addition, this LSPR sensor is insensitive to the temperature change, presenting a great potential in practical applications.

Keywords: localized surface plasmon resonance; fiber-optic LSPR sensors; supercapacitor; state of charge monitoring.

***Corresponding authors: Jie Zhu,** Research Center for Fluid-Structure Interactions, Department of Mechanical Engineering, Hong Kong Polytechnic University, Hong Kong SAR, China, e-mail: jiezhu@polyu.edu.hk. https://orcid.org/0000-0002-2547-7775; and **Shengchun Liu,** Heilongjiang Provincial Key Laboratory of Metamaterials Physics and Device, Heilongjiang University, Harbin 150080, China, e-mail: Liushengchun@hlju.edu.cn
Siyu Qian, Xinlong Chen, Shiyu Jiang and Yachen Gao: Heilongjiang Provincial Key Laboratory of Metamaterials Physics and Device, Heilongjiang University, Harbin 150080, China
Qiwen Pan and Lei Wang: Key Laboratory of Functional Inorganic Material Chemistry, Ministry of Education of the People's Republic of China, Heilongjiang University, Harbin 150080, China
Wei Peng: College of Physics and Optoelectronics Engineering, Dalian University of Technology, Dalian 116024, China
Shanjun Liang: Research Center for Fluid-Structure Interactions, Department of Mechanical Engineering, Hong Kong Polytechnic University, Hong Kong SAR, China; and Division of Science, Engineering and Health Studies, College of Professional and Continuing Education, Hong Kong Polytechnic University, Hong Kong SAR, China

1 Introduction

With the rapid growth of global energy demand, the development of highly efficient and environmentally friendly energy storage devices is essential for better energy utilization. Supercapacitors, also called as ultracapacitors, are very promising energy storage devices with high power density, high charge/discharge rates, long cycle life and simple mechanism [1, 2]. They are suitable for applications in fields such as electric vehicles, communication, electronic devices and wearable devices [3, 4]. The energy storage in pseudocapacitors shows redox reactions similar to the traditional batteries but at extremely high rates [5, 6]. Compared with conventional capacitors, the energy density in supercapacitors is several orders of magnitude higher [7]. Although the energy density is lower, supercapacitors can produce much higher power density compared with conventional batteries. In addition, supercapacitors have an ultralong lifespan ranging from 100,000 to a million cycles, compared with 500 and 10,000 cycles of lithium-ion batteries [8]. With a wide range of operating temperature, the supercapacitors can be used in extreme weather [9].

Techniques have been developed for monitoring the charge quantity and efficiency of supercapacitors and batteries [10]. For instance, Zhi's team used scanning electron microscopy (SEM) and X-ray diffraction to study the MnO_2 deposition-dissolution mechanism on carbon cloth and showed that the MnO_2-Cu battery has excellent

energy density and power density [11]. They also confirmed the Na ion and water molecules pre-interaction can effectively activate stable Zn ion storage of δ-MnO_2 [12]. Wang's group proposed an "operando" transmission electron microscopy (TEM) technique [13]. It can provide the configuration of a real battery in a relevant liquid electrolyte, which helps in understanding the electrode and the electrode-electrolyte interaction. In order to better understand the principle, Cui's group utilized cryo-electron microscopy to observe the sensitive battery materials and interfaces with atomic resolution. It can help in understanding the mechanisms, especially the reason of failure in a high-energy battery [14]. Other methods, such as infrared spectroscopy [15], Raman spectroscopy [16], and nuclear magnetic resonance [17], were used in *in situ* monitoring the electrode. Although the methods mentioned above can achieve good results, the instrument setups are expensive, bulky and complicated; therefore, they cannot meet the goal of portable monitoring of the electrode and charge/discharge process in the supercapacitor and battery.

During the charging and discharging process in the supercapacitor, ion migration causes the refractive index (RI) change near the electrode. Localized surface plasmon resonance (LSPR) is sensitive to the RI change and leads to the wavelength's intensity shift in the resonance spectrum [18]. LSPR occurred when the frequencies of incident photons match the collective oscillation of electrons at the surface of metallic nanoparticles [19, 20]. The optical extinction is in accordance with plasmonic resonance frequency [21]. Compared with lens-based LSPR sensors, fiber-optic based LSPR sensors are more flexible; the lower cost and smaller size are suitable for portable sensing [22, 23]. Thus, the fiber-optic LSPR sensors have great potential in implantation monitoring and *in situ* monitoring [24–26]. Unlike surface plasmon resonance (SPR) technology where the signal fluctuates greatly when the ambient temperature changes [27], LSPR sensor is insensitive to the change of surrounding temperature [28] and more suitable of being implanted in the supercapacitor for online monitoring. Guo's group used a novel tilted fiber Bragg grating (TFBG) based SPR sensor for monitoring the battery charging and discharging process. The Bragg resonance in the fiber core can overcome the temperature cross-interference issue. However, the TFBG fiber still needs special equipment for elaborated fabrication.

In this paper, we present a multimode fiber-optic based LSPR sensor, which does not require special equipment and is easy to fabricate. It can be implanted in a supercapacitor for *in situ* monitoring of MnO_2 growth on the electrode and the state of charge in the charge-discharge process. In a cyclic voltammetry (CV) test, the intensity shift of the LSPR spectrum clearly reflects the charge and discharge process and real-time quantity of the supercapacitor charge. The highest intensity shift of LSPR signal is proportional in accordance with the state of charge on the MnO_2 electrode calculated in a galvanostatic test. Compared with the electrochemical method of measuring the quantity of charge by integration, the fiber-optic LSPR sensor is able to detect and demonstrate the state of charge in real time. Finally, the sensor performance is measured at different temperatures to test its reliability in the supercapacitor.

2 Fabrication and experiments

2.1 AuNPs preparation

The Au nanoparticles (AuNPs) were synthesized by sodium citrate reduction method [29]. Before the experiment, all glassware was thoroughly immersed in aqua regia (HCl: HNO_3 = 3:1) for 30 min then rinsed with deionized water and dried. In 250 ml round bottom flasks, 1 ml of 1% $HAuCl_4$ and 100 ml deionized water were mixed and heated to boiling under vigorous stirring. Then, 1.2 ml of 1% sodium citrate aqueous solution was rapidly added, and boiling was continued for 15 min. During this process, the mixture solution gradually turned red. The sodium citrate reduction method synthesized AuNPs was negatively charged. The average diameter of AuNPs was 40 nm as calculated by UV-Vis absorption spectrum (Figure S2) [30].

2.2 LSPR sensing probe fabrication

The schematic illustration structure of fiber-optic LSPR sensors is shown in Figure 1. The multimode fiber is used for sensing with 600 μm core diameter and 0.37 numerical aperture. The length of the sensing fiber is cut to 7.5 cm.

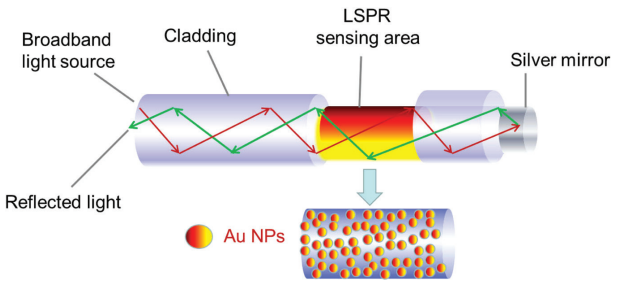

Figure 1: Schematic illustration of fiber-optic LSPR sensing probe.

The jacket and cladding are removed from the end of the optical fiber for 2 mm to load a silver reflective mirror. In the sensing region, 10 mm length of jacket and cladding are removed for loading AuNPs for the sensing purpose. The exposed fiber probe is cleaned and hydrolyzed with piranha solution at 65°C for 30 min to form a hydrophilic layer on the unclad fiber. The piranha solution is a mixture of H_2SO_4 and H_2O_2 with 3:1 in volume ratio.

The unclad sensing fiber is then immersed in 10% (v/v) 3-aminopropyltriethoxysilane aqueous solution for 1 h and rinsed in ethanol with sonication. The fiber needs to stay in a drying oven at 120°C for 2 h. By treating the surface with silane, the hydrophilic region of the unclad fiber is functionalized with an amino group. The unclad fiber is subsequently immersed into 40 nm AuNPs solution for 3 h. The negative charged AuNPs can attach to the amino group functionalized unclad fiber core through electrostatic interaction force. The immobilization of AuNPs on the fiber core can be confirmed by using the field emission SEM (SIGMA500).

The end point of the fiber is coated with silver as the reflective layer by Tollens's reaction. To do it, the fiber is firstly held in a small bottle. One milliliter 0.5 mol/l $AgNO_3$ solution is added to the small bottle. Then, the 6 mol/l ammonia solution is added, too. The solution turns brown first and later becomes clear and transparent. A few drops of 30% glucose solution is added, and the sample is kept in 70°C for 30 min to form a silver layer on the end face of the fiber. Epoxy resin ab glue was used to cover the silver mirror to protect it and prevent the SPR signal in the silver reflective film.

2.3 Fiber-optic LSPR sensing system

The AuNP-coated optical fiber with a core diameter of 600 μm is connected with Y-type fiber jumper by an SMA 905 coupler. The Y-type of jumper has two legs with 200 μm core diameter. One leg is connected to the halogen light source (HL-2000), the other one is connected to the spectrometer (Ocean Optics HR4000, Rochester, NY, USA). The incident light is coupled to the LSPR probe to stimulate the LSPR. The reflected light can be received and sent to the spectrometer for data processing and analysis with LabVIEW platform.

2.4 Construction of supercapacitor and *in situ* charge monitoring system

The MnO_2 electrode is synthesized by electrochemical deposition [31]. Briefly, the Mn ions electrolyte is made of 0.1 M $MnAc_2$ and 0.1 M $NaAc_2$. The carbon fabric is boiled in ethanol for 30 min and ultrasonicated in 1 M HCl solution for 30 min. Then the carbon fabric (area 1 * 2 cm) is immersed in Mn ions electrolyte. The three-electrode system can be used for MnO_2 fabrication on the carbon fabric with Ag/AgCl as reference electrode and Pt as the counter electrode. The constant current is 1 mA/cm^{-2} in anodic for 5 min. The fiber-optic LSPR sensor is firstly used to monitor the MnO_2 growth process on the carbon fabric. The instrument setup of fiber-optic LSPR sensor is similar to the charge and discharge process monitoring in supercapacitor. The MnO_2-coated carbon fabric is rinsed with water and dried overnight in 60°C oven before use.

To monitor the state of charge change during the charge and discharge process near the MnO_2 electrode, the fiber-optic LSPR sensing probe is implanted in the supercapacitor. As shown in Figure 2B, we use the three-electrode system to form the supercapacitor with MnO_2 on carbon fabric as working electrode, Ag/Ag/Cl as reference electrode and Pt as the counter electrode. The electrolyte is 1 M LiCl. The tiny fiber-optic LSPR sensor is hooked near the MnO_2 electrode by a microporous membrane. Due to the short LSPR sensing distance, the fiber-optic LSPR sensing region must be closely attached to the electrode.

3 Results and discussion

3.1 Characterization of fiber-optic LSPR sensor

A SEM image of the sensing region is shown in Figure 2C. The sensing region coated with AuNPs was 1 cm. The image shows that the AuNPs are successfully and uniformly attached on the fiber core. The AuNP-coated fiber-optic probe is stable in the neutral LiCl electrolyte during the charging and discharging process.

To verify the sensitivity and stability of the AuNP-coated fiber-optics LSPR sensor, we place the fiber probe into NaCl solutions with different RI which are measured with an Abbe refractometer to be 1.3327 (water), 1.3406, 1.3480, 1.3550, 1.3614 and 1.3671. As shown in Figure 3A, the resonance wavelength changes for fiber-optic LSPR sensors in NaCl solutions with different RI. The resonance wavelength and intensity changes in fiber-optic LSPR when exposed to different NaCl solutions are recorded in Figure 3B. Figure 3A and B show that, with the increase of RI, the intensity of fiber-optic LSPR

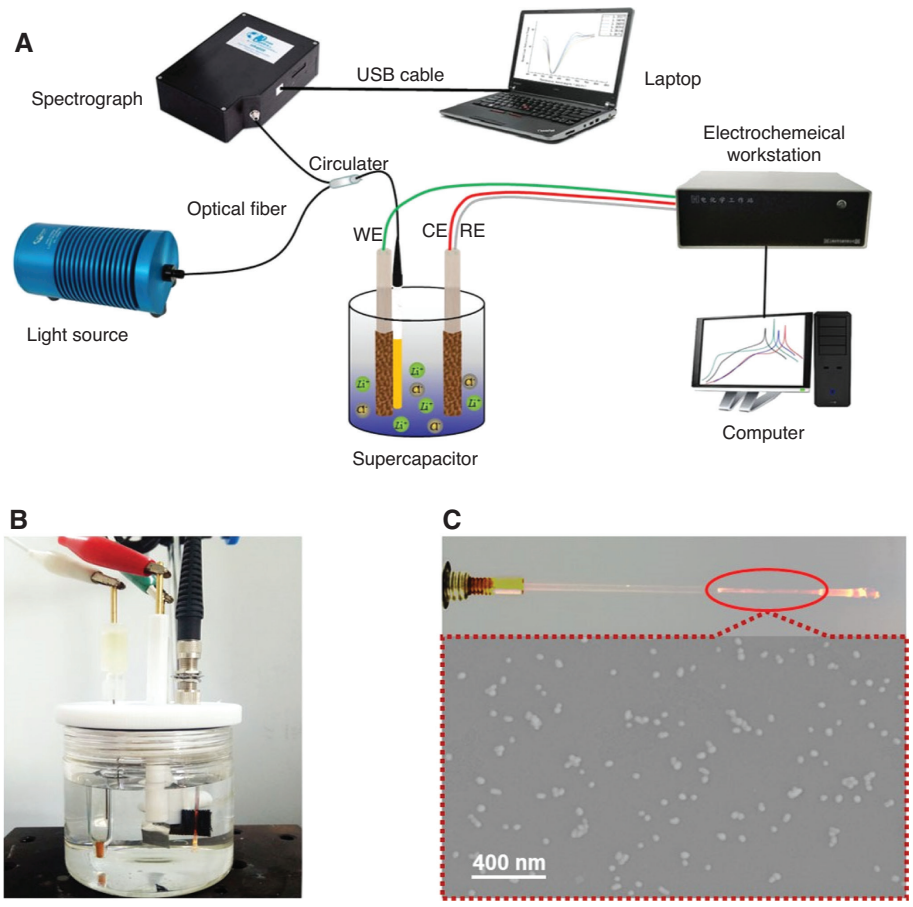

Figure 2: Fiber-optic LSPR sensor for *in situ* monitoring the state of charge in supercapacitor.
(A) Schematic representation of instrumental sensing system for fiber-optic LSPR sensor monitoring the charge and discharge process in supercapacitor. (B) The picture of *in situ* monitoring supercapacitor with fiber-optic LSPR sensor. (C) Optical and SEM image of sensing surface of the fiber-optic LSPR sensor.

sensor drops significantly. The intensity shift is measured as the % depth. The sensitivity for intensity modulation is 314.7%/RIU. A plot of the LSPR wavelength shift as a function of the RI value change in Figure 3C shows that the sensitivity for wavelength modulation is 94.5 nm/RIU. Both intensity shift and wavelength shift are linear with RI change. This test shows that the fiber-optic LSPR sensors can accurately monitor the surrounding RI change. The sensitivity for intensity modulation is much higher than the wavelength modulation in LSPR sensors.

3.2 MnO_2 growth process monitoring on the electrode

In general, supercapacitors can be categorized into two types. One is electric double-layer capacitor, which generates an electrical field between two parallel conductor plates. The other is pseudocapacitor, which stores the energy by transferring electrons between electrode and electrolyte through electrochemical reaction. The carbon fabric-based MnO_2 electrode can be used in a pseudocapacitor, which has high surface area and high specific capacitance. The electrochemical deposition technique was used to load the multiporous MnO_2 on carbon fabric.

Interestingly, we find that when the fiber-optic LSPR probe is attached near the surface of the carbon fabric, it has superior capability of monitoring the MnO_2 fabrication process. In addition, it will not disturb the MnO_2 growth on the carbon fabric. Figure 4A shows that when 1 mA/cm^2 current is applied on the working electrode, the intensity of the plasmon resonance peak will increase accordingly. As time goes on, the intensity shift tends to be flat. After 5 min of electrodeposition, MnO_2 on the carbon fabric will be saturated without the requirement of further extension. In Figure 4B, the carbon cloth

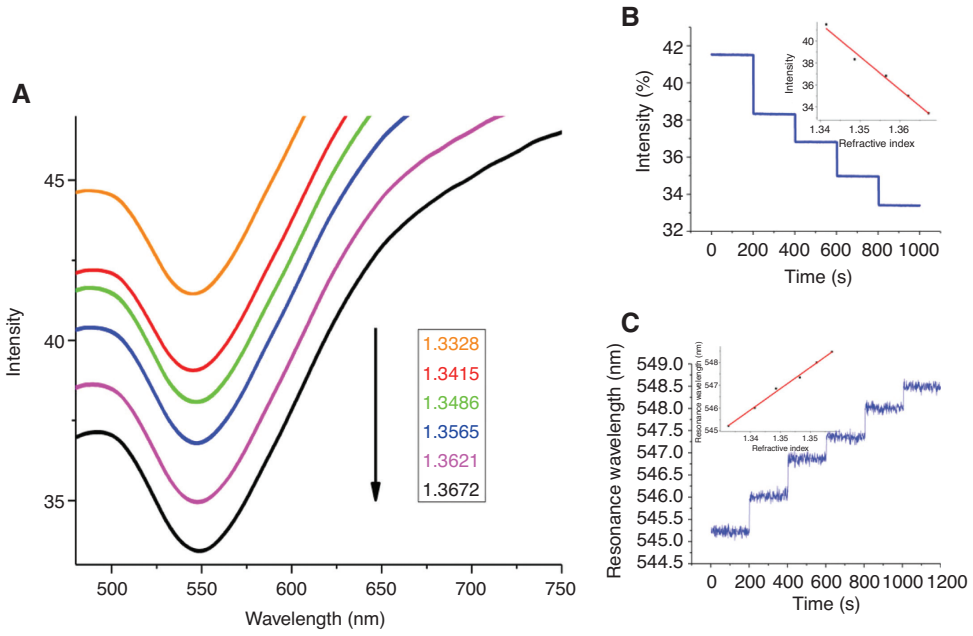

Figure 3: RI tests for fiber-optic LSPR sensors.
(A) The resonance wavelength changes of fiber-optic LSPR sensors in NaCl solutions with different RI. (B) Intensity shift with RI change in solutions. (C) Wavelength shift with RI change in solutions.

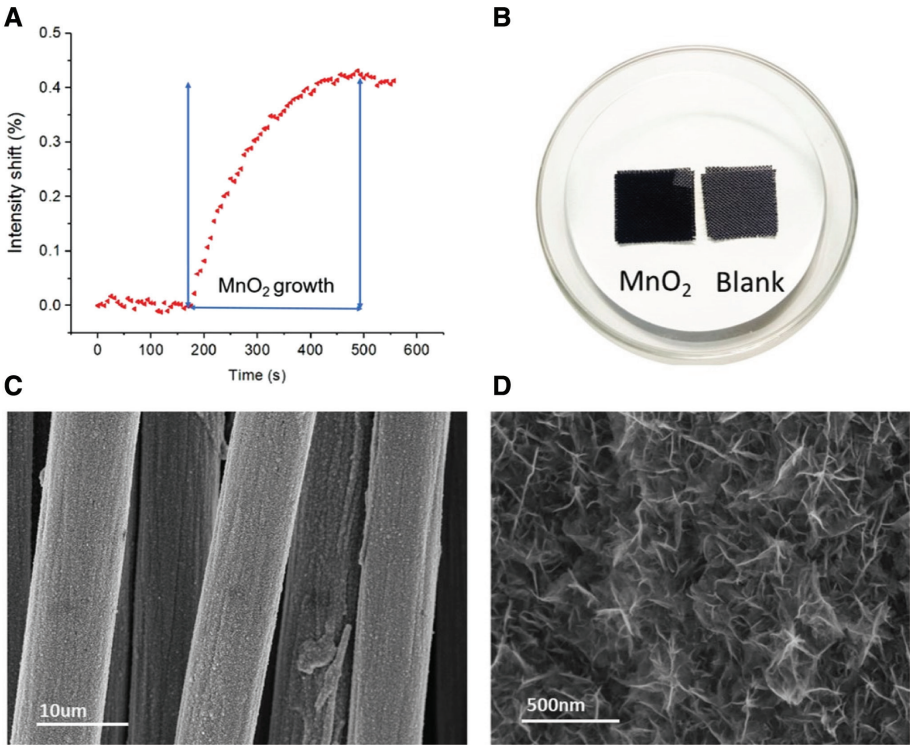

Figure 4: MnO_2 growth on carbon fabric.
(A) On-line monitoring MnO_2 growth process on carbon fabric by fiber-optic LSPR sensor (B) MnO_2 loaded carbon fabric (left), the blank fabric (right). (C) SEM image of MnO_2 on carbon fabric. (D) Magnified SEM image of MnO_2 on carbon fabric.

loaded with MnO_2 demonstrates a black color, while the blank carbon fabric is gray. The electrode with MnO_2 is darker. Figure 4C and D is the SEM image of the surface of carbon fabric loaded with MnO_2. The MnO_2 was successfully loaded and uniformly grown on the carbon fabric in floccus morphology.

3.3 State of charge monitoring in CV test

The online monitoring of the charging/discharging process in the supercapacitor can be accomplished by the proposed fiber-optic LSPR sensors. Compared with SPR sensors, LSPR sensors are insensitive for the temperature fluctuation, making it more suitable for supercapacitor monitoring. Besides, the fiber-optic LSPR sensors with tiny size and electromagnetic immunity can be implanted in the supercapacitor for *in situ* monitoring. During the charging process, ions in the electrolyte can be gathered around the polyporous MnO_2 electrode which causes the RI change near the electrode. The ion concentration around the MnO_2 electrode is proportional to the amount of charge in the supercapacitor. Hence, by monitoring the ion concentrations near the electrode by fiber-optic LSPR sensor, we can detect the real-time state of charge in the supercapacitors.

Figure 5A shows the CV curves at different scan rates. The upper part of the CV curve represents the charging process, and the lower part of the CV curve represents the discharging process in the supercapacitor. The CV integral area is the capacitance of the electrode. Figure 5B shows the real-time intensity shift of fiber-optic LSPR sensors. It demonstrates the real-time state of charge on the electrode. However, the CV curve can only calculate the whole capacity when the whole period scan was ended. It cannot detect the real-time capacity change. By contrast, the fiber-optic LSPR sensor we proposed can monitor the state of charge in supercapacitors in real time, instead of just a "calculated capacity" by CV curve. At 10 mV/S, 15 mV/S and 20 mV/S, the highest intensity shift ($\%_{max}$) is 0.238, 0.160 and 0.134, respectively, which is consistent with the result in CV curves.

3.4 State of charge monitoring in galvanostatic test

Figure 6A shows the galvanostatic charge-discharge curves of MnO_2 electrode with different constant current (0.5 mA, 1.0 mA and 2.0 mA). The charge-discharge curve is relatively symmetrical, indicating that the redox reaction on the electrode is reversible and the capacitive characteristic is steady. The high voltage was fixed at 0.8 V and the change is plotted in potential versus time at a constant rate. When the current is smaller, more charge can accumulate in and around the MnO_2 electrode. Hence, the 0.5 mA current can achieve the highest stored charge, while the 2.0 mA current produces the lowest stored charge. The real-time monitored charge density by fiber-optic LSPR sensor is shown in Figure 6B. It agrees well with the galvanostatic test result: the lower current leads to higher intensity shift of LSPR probe, and the higher one gives the lower intensity shift. The peak value of intensity shift can reflect the charge amount at the time of full charge. The signal duration in the LSPR sensor is the same with the time duration in the galvanostatic charge and discharge test. Compared with offline stored charge detection by galvanostatic test, the fiber-optic LSPR sensor can realize online monitoring of the state of charge at any time in each test. In order to confirm whether the intensity shift in the LSPR signal can accurately monitor the state of charge on the electrode, a linear fit of the relationship between the capacitance (C) and the highest intensity shift ($\%_{max}$) can be made as shown in Figure 6C. The fitted linear curve is as follows: $\%max = 0.004 \times C + 0.118$ ($R^2 = 98.5\%$). And the state of charge sensitivity of fiber-optic LSPR sensors is 3.2×10^{-3} %/mC. At each constant current, the test was made three times.

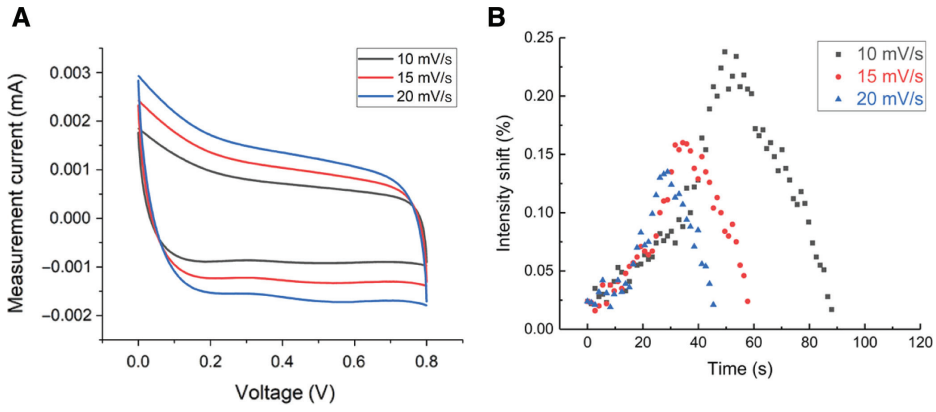

Figure 5: Charge and discharge tests in CV mode.
(A) CV curves for MnO_2 electrode at different scan rates. (B) Real-time intensity shift of fiber-optic LSPR sensors at different scan rates in CV test (10 mV/S, 15 mV/S, 20 mV/S).

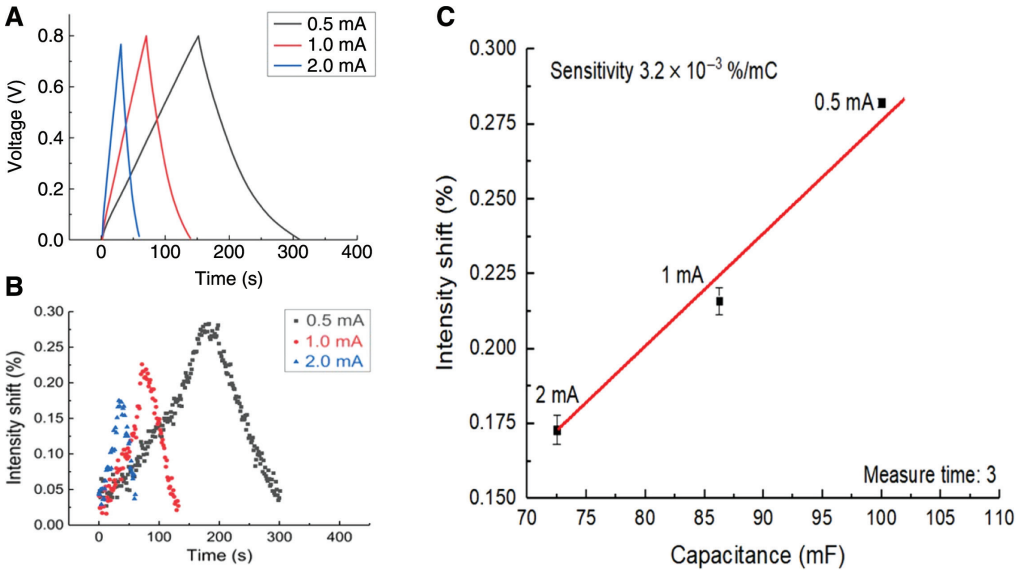

Figure 6: Charge and discharge tests in galvanostatic mode.
(A) Galvanostatic charge-discharge curve at different constant current. (B) Real-time intensity shift of fiber-optic LSPR sensors at different constant current in galvanostatic test. (C) Linear fitting curve between the intensity shift (%) in fiber-optic LSPR sensor and calculated capacitance at different constant current (0.5 mA, 1.0 mA, 2.0 mA).

3.5 Temperature influence test

The temperature test of the supercapacitor with an implanted LSPR sensing probe has been conducted in a programmable temperature and humidity chamber at different temperatures and constant humidity. All the galvanostatic charge-discharge tests are performed at 0.5 mA. Figure 7A shows that both of the charging and discharging time increase with temperature, which means that more charges accumulate on the sensing surface. At 25°C, 35°C and 45°C, the capacitance is 112.0 mF, 119.7 mF and 132.2 mF, respectively. And the capacitance and state of charge in the supercapacitor grew at 0.958 mF/°C and 0.767 mC/°C, respectively. In accordance with the result in the galvanostatic curve, the signal of intensity shift in fiber-optic LSPR sensor increases proportionately as well (Figure 7B).

A tendency relationship of stored charge shift calculated by galvanostatic curve and highest intensity shift

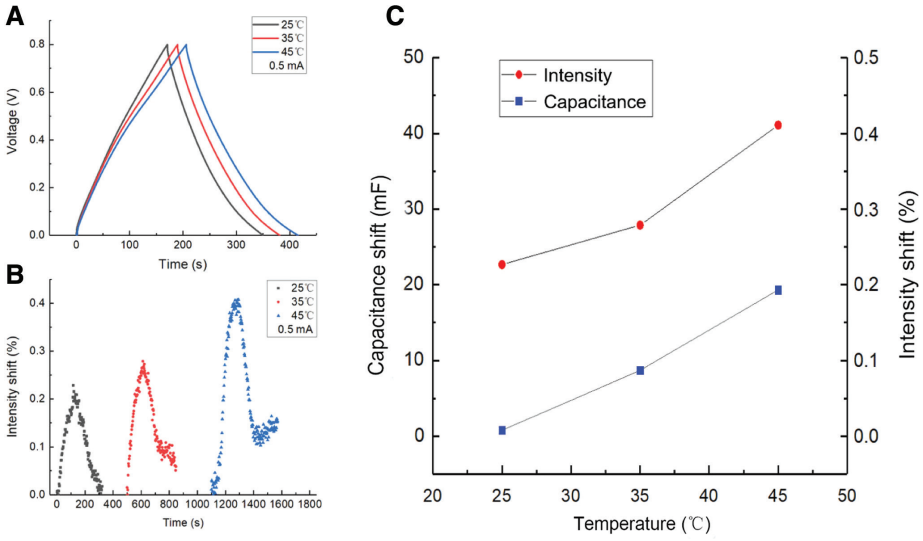

Figure 7: Charge and discharge tests of supercapacitor at different working temperature.
(A) Galvanostatic charge-discharge curve at different temperature (0.5 mA). (B) Real-time intensity shift of fiber-optic LSPR sensors at different temperature in galvanostatic test (0.5 mA). (C) The capacitance shift calculated by galvanostatic curve and LSPR intensity shift in different temperature (25°C, 35°C, 45°C).

of LSPR sensors is plotted at different temperatures. In Figure 7C, the standard stored charge shift can be calculated by the galvanostatic charge-discharge curve. The intensity shift of LSPR sensors can precisely reflect the stored charge on the electrode at different temperatures. Thence, this result can confirm that the signal of fiber-optic LSPR sensor is insensitive to the surrounding temperature. Even under temperature fluctuations, the fiber-optic LSPR sensor can still accurately conduct online monitoring of the stored charge on the electrode.

4 Conclusion

With the presented work, we demonstrate that the fiber-optic LSPR sensor can be used in real-time online monitoring of the state of charge in the supercapacitor. It was firstly used to monitor the MnO_2 growth process and the stored charge on the electrode in the pseudocapacitor. In the CV test with different scan rates, the intensity shift of the LSPR sensors is found to be proportional to the stored charge calculated by the CV curve. In addition, it also can reflect the charging-discharging process directly. In the galvanostatic test, the intensity shift of the LSPR spectrum has a relatively good linear relationship with the state of charge calculated at different constant currents by standard electrochemical method. The state of charge sensitivity is 3.2×10^{-3}%/mC. The charge detection in the supercapacitor was also conducted at different temperatures. The result shows that temperature changes have little effect on charge detection by the fiber-optic LSPR sensors.

Compared with techniques such as TEM, nuclear magnetic resonance and X-ray Raman scattering, the fiber-optic LSPR sensor is tiny in size and cost-effective, so that it can be implanted in the supercapacitor to monitor the charging-discharging process. It promises great potential in monitoring the state of charge *in situ* for application targets such as electric vehicles or other electronic instruments.

Acknowledgments: This research was financially supported by the Hong Kong Research Grants Council under Contract No. PolyU152119/18E, Funder Id: http://dx.doi.org/10.13039/501100002920 and the National Nature Science Foundation of China (61905069, 11774081, 61575061, and 61520106013, Funder Id: http://dx.doi.org/10.13039/501100001809). The authors also acknowledge support from the Outstanding Youth Science Foundation of Heilongjiang University under Grant JCL201606 and Heilongjiang Province Postdoctoral Fund LBH-Z19092.

References

[1] Yang P, Li Y, Lin Z, et al. Worm-like amorphous MnO2 nanowires grown on textiles for high-performance flexible supercapacitors. J Mater Chem A 2014;2:595–9.
[2] Ji L, Gu M, Shao Y, et al. Controlling SEI formation on SnSb-porous carbon nanofibers for improved Na ion storage. Adv Mater 2014;26:2901–8.
[3] Castaings A, Lhomme W, Trigui R, Bouscayrol A. Comparison of energy management strategies of a battery/supercapacitors system for electric vehicle under real-time constraints. Appl Energ 2016;163:190–200.
[4] Burke A. Ultracapacitor technologies and application in hybrid and electric vehicles. Int J Energ Res 2010;34:133–51.
[5] Costentin C, Porter TR, Savéant JM. How do pseudocapacitors store energy? Theoretical analysis and experimental illustration. ACS Appl Mater Inter 2017;9:8649–58.
[6] Lesel BK, Ko JS, Dunn B, Tolbert SH. Mesoporous $LixMn_2O_4$ thin film cathodes for lithium-ion pseudocapacitors. ACS Nano 2016;10:7572–81.
[7] Lu X, Yu M, Wang G, Tong Y, Li Y. Flexible solid-state supercapacitors: design, fabrication and applications. Energ Environ Sci 2014;7:2160–81.
[8] Shah V, Joshi JA, Maheshwari R, Roy R. In review of ultracapacitor technology and its applications, Proceedings of the 15th National Power System Conference, Mumbai, India. 2008:142–7.
[9] Tani A, Camara MB, Dakyo B. Energy management in the decentralized generation systems based on renewable energy – ultracapacitors and battery to compensate the wind/load power fluctuations. IEEE Trans Ind Appl 2015;51:1817–27.
[10] Liu D, Shadike Z, Lin R, et al. Review of recent development of in situ/operando characterization techniques for lithium battery research. Adv Mater 2019;31:1806620.
[11] Liang G, Mo F, Li H, et al. A universal principle to design reversible aqueous batteries based on deposition-dissolution mechanism. Adv Energ Mater 2019;9:1901838.
[12] Wang D, Wang L, Liang G, et al. A superior δ-MnO_2 cathode and a self-healing Zn-δ-MnO_2 battery. ACS Nano 2019;13:10643–52.
[13] Gu M, Parent LR, Mehdi BL, et al. Demonstration of an electrochemical liquid cell for operando transmission electron microscopy observation of the lithiation/delithiation behavior of si nanowire battery anodes. Nano Letters 2013;13:6106–12.
[14] Li Y, Li Y, Pei A, et al. Atomic structure of sensitive battery materials and interfaces revealed by cryo-electron microscopy. Science 2017;358:506–10.
[15] Dillard C, Singh A, Kalra V. Polysulfide speciation and electrolyte interactions in lithium-sulfur batteries with in situ infrared spectroelectrochemistry. J Phys Chem C 2018;122:18195–203.
[16] Dai S, Zhang Z, Xu J, et al. In situ Raman study of nickel bicarbonate for high-performance energy storage device. Nano Energy 2019;64:103919.
[17] Oukali G, Salager E, Ammar MR, et al. In situ magnetic resonance imaging of a complete supercapacitor giving additional insight on the role of nanopores. ACS Nano 2019;13:12810–5.
[18] Lu M, Zhu H, Bazuin CG, Peng W, Masson JF. Polymer-templated gold nanoparticles on optical fibers for enhanced-sensitivity localized surface plasmon resonance biosensors. ACS Sensors 2019;4:613–22.
[19] Jiang J, Wang X, Li S, et al. Plasmonic nano-arrays for ultrasensitive bio-sensing. Nanophotonics 2018;7:1517.

[20] Abdulhalim I. Coupling configurations between extended surface electromagnetic waves and localized surface plasmons for ultrahigh field enhancement. Nanophotonics 2018;7:1891.
[21] Rippa M, Castagna R, Pannico M, et al. Engineered plasmonic Thue-Morse nanostructures for LSPR detection of the pesticide Thiram. Nanophotonics 2017;6:1083.
[22] Caucheteur C, Guo T, Albert J. Review of plasmonic fiber optic biochemical sensors: improving the limit of detection. Anal Bioanal Chem 2015;407:3883–97.
[23] Sharma AK, Jha R, Gupta BD. Fiber-optic sensors based on surface plasmon resonance: a comprehensive review. IEEE Sens J 2007;7:1118–29.
[24] Chen S, Liu Y, Liu Q, Peng W. Localized surface plasmon resonance-based micro-capillary biosensor. IEEE Photonic Technol Lett 2016;28:2195–8.
[25] Jeong HH, Erdene N, Park JH, Jeong DH, Lee HY, Lee SK. Real-time label-free immunoassay of interferon-gamma and prostate-specific antigen using a fiber-optic localized surface plasmon resonance sensor. Biosens Bioelectron 2013;39:346–51.
[26] Lee B, Park JH, Byun JY, Kim JH, Kim MG. An optical fiber-based LSPR aptasensor for simple and rapid in-situ detection of ochratoxin A. Biosens Bioelectron 2018;102:504–9.
[27] Homola J. Surface plasmon resonance sensors for detection of chemical and biological species. Chem Rev 2008;108:462–93.
[28] Willets KA, Duyne RPV. Localized surface plasmon resonance spectroscopy and sensing. Annu Rev Phys Chem 2007;58:267–97.
[29] Qian S, Lin M, Ji W, et al. Boronic acid functionalized Au nanoparticles for selective microRNA signal amplification in fiber-optic surface plasmon resonance sensing system. ACS Sensors 2018;3:929–35.
[30] Haiss W, Thanh NTK, Aveyard J, Fernig DG. Determination of size and concentration of gold nanoparticles from UV-Vis spectra. Anal Chem 2007;79:4215–21.
[31] Lao J, Sun P, Liu F, et al. In situ plasmonic optical fiber detection of the state of charge of supercapacitors for renewable energy storage. Light Sci Appl 2018;7:34.

Supplementary Material: The online version of this article offers supplementary material (https://doi.org/10.1515/nanoph-2019-0504).